

1 **Surprising variation in the outcome of two malaria genetic crosses using humanized mice:**
2 **implications for genetic mapping and malaria biology**

3
4 Katrina A. Button-Simons¹, Sudhir Kumar², Nelly Carmago², Meseret T. Haile², Catherine Jett³,
5 Lisa A. Checkley¹, Spencer Y. Kennedy², Richard S. Pinapati⁴, Douglas A. Shou¹, Marina
6 McDew-White⁵, Xue Li⁵, François H. Nosten^{6,7}, Stefan H. Kappe², Timothy J. C. Anderson⁵,
7 Jeanne Romero-Severson⁸, Michael T. Ferdig¹, Scott J. Emrich⁹, Ashley M. Vaughan², Ian H.
8 Cheeseman^{3*}

9
10 ¹*Eck Institute for Global Health, Department of Biological Sciences, University of Notre Dame,*
11 *Notre Dame, IN, USA*

12 ²*Center for Global Infectious Disease Research, Seattle Children's Research Institute, Seattle,*
13 *WA, USA*

14 ³*Host-Pathogen Interactions Program, Texas Biomedical Research Institute, San Antonio, TX,*
15 *USA*

16 ⁴*Nimble Therapeutics, Madison, WI*

17 ⁵*Disease Intervention and Prevention Program, Texas Biomedical Research Institute, San*
18 *Antonio, TX, USA*

19 ⁶*Shoklo Malaria Research Unit, Mahidol-Oxford Tropical Medicine Research Unit, Mahidol*
20 *University, Mae Sot, Thailand*

21 ⁷*Centre for Tropical Medicine and Global Health, Nuffield Department of Medicine Research*
22 *building, University of Oxford Old Road campus, Oxford, UK*

23 ⁸*Department of Biological Sciences, University of Notre Dame, IN*

24 ⁹*Univeristy of Tennessee, Knoxville, TN, USA*

25

26 * Corresponding author

27 E-mail: ianc@txbiomed.org

28

29 **Abstract**

30 Genetic crosses are most powerful for linkage analysis when progeny numbers are high,
31 when parental alleles segregate evenly and, for hermaphroditic organisms, when numbers of
32 inbred progeny are minimized. We previously developed a novel genetic crossing platform for
33 the human malaria parasite *Plasmodium falciparum*, an obligately sexual, hermaphroditic
34 protozoan, using mice carrying human hepatocytes (the human liver-chimeric FRG NOD huHep
35 mouse) as the vertebrate host. Here we examine the statistical power of two different genetic
36 crosses – (1) between a laboratory parasite (NF54) of African origin and a patient-derived Asian
37 parasite, and (2) between two sympatric patient-derived Asian parasites. We generated >140
38 unique recombinant clones over a 12-month period from the four parental genotypes, doubling
39 the number of unique recombinant progeny generated in the previous 30 years. Both crosses
40 show bi-parental inheritance of plastid markers amongst recombinant progeny, in contrast to
41 previous crosses (conducted using chimpanzee hosts) which carried single dominant plastid
42 genotypes. Both crosses show distinctive segregation patterns. The allopatric African/Asian cross
43 has minimal levels of inbreeding (2% of clonal progeny are inbred) and extreme skews in marker
44 segregation, while in the sympatric Asian cross, inbred progeny predominate (66% of clonal
45 progeny are inbred) and parental alleles segregate evenly. Using simulations, we demonstrate
46 that these progeny arrays (particularly the sympatric Asian cross) have excellent power to map

47 large-effect mutations to a 31 kb interval and can capture complex, epistatic interactions that
48 were far beyond the capacity of previous malaria crosses to detect. The extreme segregation
49 distortion in the allopatric African/Asian cross erodes power to detect linkage in several genome
50 regions, but the repeatable distortions observed offer promising alternative approaches to
51 identifying genes underlying traits of interest. These crosses show surprising variation in marker
52 segregation, nevertheless, the increased progeny numbers improve our ability to rapidly map
53 biomedically important parasite traits.

54

55 **Author Summary**

56 Understanding how genome mutations contribute to newly emerging drug resistance in
57 parasites like *Plasmodium falciparum* is important to monitor the spread of drug resistance. This
58 scenario has been playing out in Southeast Asia with the emergence and spread of artemisinin
59 resistance. Here we show that new *P. falciparum* genetic crosses, using mice carrying human
60 liver cells and infused with human red blood cells (the human liver-chimeric FRG NOD
61 huHep/huRBC mouse), provide an important new tool for understanding complex interactions
62 underlying drug resistance phenotypes. We report two new genetic maps with 84 and 60 unique
63 recombinant progeny, which doubles the number of progeny available from 4 previous *P.*
64 *falciparum* genetic crosses. Through extensive simulations we show that with 84 progeny we can
65 find association for a gene that controls only 20% of the variation in a phenotype. We also show
66 that a cross generated from Southeast Asian parasites collected from the same geographic region
67 have unique characteristics not previously observed in *P. falciparum* genetic crosses. This
68 Southeast Asian cross exhibits even segregation across the genome, unbiased inheritance of
69 mitochondria and apicoplast and higher levels of inbreeding than previously observed.

70

71 **Introduction**

72 Eukaryotic parasites inflict a high burden of morbidity and mortality particularly in the
73 developing world. Control of these pathogens is threatened by drug resistance [1, 2].
74 Understanding the genetic architecture of drug resistance in eukaryotic pathogens is essential to
75 understand treatment failure. Previous studies in Plasmodium, Trypanosome and Leishmania
76 parasites revealed the genetic architecture of drug resistance is unexpectedly complex [3-6]. For
77 example, emergent artemisinin resistance in the human malaria parasite, *Plasmodium*
78 *falciparum*, has been causally associated with multiple independent mutations in one gene,
79 *pfK13*, which explain nearly all the variation in this phenotype [7-9]. However, mutations in the
80 *pffd*, *pfarps10*, *pfmdr2*, and *pfcr1* genes are significantly associated with resistance, and have
81 been proposed to constitute a genetic background highly predisposed to the development of
82 resistance [7]. Several techniques have been used to identify the genetic determinants of complex
83 phenotypes in eukaryotic pathogens including GWAS [7, 10], *in vitro* selections [8], QTL
84 analysis in controlled genetic crosses [11-14] and bulk segregant analysis [5, 15]. Controlled
85 genetic crosses offer a uniquely powerful way to dissect the genetic architecture of a complex
86 trait. For example, the F₁ progeny of a controlled cross revealed that *P. falciparum* sensitivity to
87 quinine was associated with loci on chromosomes 5, 7 and 13, with the chromosome 5 and 7 loci
88 containing known drug resistance transporters *pfcr1* and *pfmdr1* [3].

89 *P. falciparum* has the potential to be a particularly powerful genetic mapping system because
90 of its unusually high recombination rate of 11-13.3 kb/cM [13, 16, 17], a haploid state for most
91 of the life cycle, and the ability to clone every F₁ progeny *in vitro*, creating effectively immortal
92 mapping populations in a single generation. Also, *P. falciparum* has a small genome (23 Mb) and

93 a high-quality reference assembly [18] with frequent annotation updates [19, 20]; consequently,
94 re-sequencing and comprehensive analysis of the genome of F₁ progeny is simple and cost
95 effective [21]. Generating controlled genetic crosses in *P. falciparum*, however, has historically
96 been a difficult and time-consuming process requiring splenectomized chimpanzees in place of a
97 human host. This has resulted in only four genetic crosses being performed over a thirty-year
98 period. F₁ mapping populations from all four previous *P. falciparum* genetic crosses have been
99 small, containing 33, 35, 15 [21] and most recently 27 individual recombinant progeny [13].
100 When compared to the thousands of F₁ progeny possible in many plants and fruit flies [22], these
101 numbers are small indeed. To use genetic mapping to elucidate the genetic architecture of
102 emerging drug resistance in *P. falciparum* we need to be able to rapidly create genetic crosses
103 with large numbers of progeny from recent field isolated parasites which exemplify highly
104 relevant clinical traits such as drug resistance.

105 Here we report the production of large numbers of unique recombinant progeny from human
106 liver-chimeric FRG huHep mice infused with human red blood cells. Although these mice were
107 previously reported as an option for producing new *P. falciparum* genetic crosses once
108 chimpanzee research was discontinued [23], until now they have failed to produce more progeny
109 than historic crosses. In this paper, we successfully produced two new genetic crosses in under
110 twelve months using recent clinically derived *P. falciparum* isolates with emerging resistance
111 phenotypes. This effort was aided by a new progeny characterization bioinformatics framework
112 that filters SNP variants and identifies clonal unique recombinant progeny. We generate genetic
113 maps for each cross (84 and 60 unique recombinant progeny, respectively) and provide the most
114 detailed investigation of inbreeding, plastid inheritance, and cross-over rates in malaria parasite
115 genetics to date. One cross exhibited abundant segregation distortion. We confirm this is

116 repeatable by independently replicating the genetic cross, and exclude a fluorescent marker
117 integrated into genome of one parent as the cause. Through simulation and mapping with real
118 data we investigate the power to detect genetic associations as a function of the number of
119 progeny. We also examine the effect of segregation distortion on power in mapping a phenotype
120 in a cross with varying levels of segregation distortion.

121

122 **Results**

123 **Rapid Generation of Genetic Crosses**

124 Over a 12-month period we carried out two independent genetic crosses. The first
125 between a laboratory-adapted African line (NF54) and a newly cloned clinical isolate
126 (NHP4026) from the Thai-Myanmar border, the second between two newly cloned clinical
127 isolates (MKK2835 and NHP1337) from the Thai-Myanmar border. These crosses yielded 84
128 and 60 clonal unique recombinant progeny lines respectively. The pipeline to the point of
129 analyzing recombinant progeny is technically challenging and takes approximately six months
130 (Fig 1). Initially, we confirmed that the clinical isolate parental lines produced infectious
131 gametocytes that gave rise to infectious sporozoites that could the successfully infect the liver of
132 human hepatocyte-chimeric FRG NOD huHep mice and subsequently transition to *in vivo* and
133 then *in vitro* blood stage culture. After this confirmation, the steps to successfully complete a
134 genetic cross includes asexual culture and expansion, gametocyte maturation, mixing of parental
135 gametocytes and transmission to mosquitoes, confirmation of successful mosquito stage
136 development, salivary gland sporozoite isolation and infection of human hepatocytes in the FRG
137 NOD huHep mouse, liver stage development, infusion of human red blood cells, the *in vivo*
138 transition from liver stage-to-blood stage, the subsequent transition to *in vitro* blood stage culture

139 coupled with cloning by limiting dilution and finally clonal expansion, confirmation of clonality
140 and genome sequencing of recombinant progeny (Fig 1).

141 In total we initiated three independent crosses using five parental genotypes (NF54-
142 GFPLuc x NHP4026, NF54WT x NHP4026 and MKK2835 x NHP1337). The second of these
143 crosses was performed to test if a GFP cassette integrated into the genome had driven a peak in
144 segregation distortion (described below). The progeny from the first crosses were combined
145 (subsequently referred to as NF54 x NHP4026) to form one genetic map (described below). We
146 set up each genetic cross by infecting multiple cages of mosquitos with mixed gametocyte
147 cultures of our parental lines (S1 Table). Details NF54-GFPLuc x NHP4026 were previously
148 published [23]. For NF54WT x NHP4026 three cages were used to infect three mice by IV
149 injection or mosquito bite (MB) (one cage per mouse). Two mice were infected by MB using
150 cages with 250 mosquitos with prevalence of 73% and 58% and median 3 oocyst/mosquito. One
151 mouse was infected by IV injection of 1 million sporozoites dissected from 250 mosquitos with
152 infection prevalence of 73% and median 6 oocysts/mosquito. Assuming no attrition in parasite
153 genotypes, and a perfect outcrossing rate this would mean that 2190 and 1740 unique
154 recombinant progeny respectively were possibly inoculated into two mice by mosquito bite and a
155 pool of 1460 unique recombinant progeny was used to infect one mouse via IV infection.
156 Similarly, for MKK2835 x NHP1337 four cages of mosquitos were infected with pools of
157 MKK2835 and NHP1337 gametocytes and the cage with the best infections (80% prevalence and
158 median 3 oocysts/mosquito) was used to infect a single mouse via IV injection with 2.7 million
159 sporozoites. We would expect a maximum of 1958 unique recombinant progeny based upon 80%
160 successful infections and a median of 3 oocysts per mosquito and 204 mosquitos.

161

162 **Numbers of Unique Recombinant Progeny**

163 In these malaria parasite crosses, the F₁ progeny are present in the blood of the infected
164 FRG NOD huHep/huRBC mouse and must be isolated by limiting dilution cloning. The progeny
165 isolated in this way are not guaranteed to be clonal because a small subset of post-dilution
166 cultures will have been initiated with more than one clone. Additionally, as the malaria parasite
167 undergoes clonal expansion in the mosquito, liver and mouse blood stream [24] we may sample
168 the same recombinant genotype more than once. Since the parents in both crosses readily
169 produce fertile male and female gametocytes it is also possible for selfed progeny to be
170 produced. We thus developed a bioinformatics pipeline to identify clonal unique recombinant F₁
171 progeny filtering out non-clonal progeny, selfed progeny and repeat sampling of the same
172 genotype (see Methods).

173 Genetic characterization of previous crosses was initially carried out with RFLP or MS
174 markers [16, 25] and unique recombinant progeny from these crosses were recently sequenced to
175 create a community resource [21]. For NF54 x NHP4026, we filtered out some non-unique
176 recombinant progeny using MS genotyping and then performed direct genome sequencing of
177 cloned parasites. For MKK2835 x NHP1337, we performed genome sequencing of all cloned
178 parasites. For each prospective progeny, sequencing reads were mapped to version 3 of the *P.*
179 *falciparum* genome [26] and SNP variants were called jointly across parents and perspective
180 progeny and filtered to contain SNPs in the 20.8 Mb core genome as defined in Miles et al. 2016
181 [21].

182 In NF54 x NHP4026, 10,472 high-quality bi-allelic SNPs (1 SNP per 2.0 kb) differentiate
183 the two parents. For this cross, 166 prospective progeny were identified during limiting dilution
184 cloning. After filtering to remove non-clonal and selfed progeny 128 recombinant progeny

185 remained (Fig 2), 84 of which were unique. In MKK2835 x NHP1337, the parent lines are
186 sympatric patient-derived Asian parasites. Despite their higher degree of relatedness we
187 identified 7,198 high-quality bi-allelic SNPs (1 SNP per 2.9 kb) that distinguish the two parents.
188 For this cross 266 prospective progeny were identified during limiting dilution cloning. Filtering
189 was performed to remove non-clonal and selfed progeny leaving 61 recombinant progeny (Fig
190 2), 60 of which were unique. We initiated multiple cloning rounds to maximize the capture of
191 unique recombinant progeny from each cross. Interestingly, across all crosses each cloning round
192 produced nearly distinct sets of recombinant progeny, with only one repeat genotype across
193 cloning rounds (Fig 2 and S1 Fig).

194

195 **Inbreeding, Outbreeding and Plastid inheritance**

196 Through our filtering process we identified stark differences in patterns of outcrossing
197 between these two crosses. The clones recovered from NF54 x NHP4026 contained few selfed
198 progeny with three selfed NF54 progeny and 0 selfed NHP4026 progeny (1.8%, 3/166 progeny
199 selfed). In contrast, in MKK2835 x NHP1337 we observed a large amount of selfing with 144
200 selfed NHP1337 progeny and five MKK2835 selfed progeny (56%, 149/266 progeny selfed; Fig
201 2). In both crosses, when cloning was initiated immediately after mouse exsanguination or within
202 five days of establishing *in vitro* culture, almost all recombinants were unique (S2 Table and S1
203 Fig). Interestingly, when cloning was initiated within five days, whether from continuous *in vitro*
204 culture or cryopreservation of bulk culture, the percentage of recombinants that were unique was
205 high (90-100% for continuous culture vs. 93% from a thawed cryopreserved bulk culture).
206 However, when cloning was initiated after 14 or 19 days of *in vitro* culture from cryopreserved

207 bulk culture, a lower percentage of unique recombinant progeny were recovered with 46% and
208 50% of recombinants identified as unique (S2 Table and S1 Fig).

209 *P. falciparum* parasites contain two plastid genomes, the mitochondria and apicoplast,
210 both of which are maternally inherited [27]. Despite *P. falciparum* being hermaphroditic, in
211 previous genetic crosses nearly all plastid genomes in the progeny originated from a single
212 parent [28, 29]. We show here that this is not the case. In each cross we observed both plastid
213 genotypes among the unique recombinant progeny. After excluding selfed genotypes we
214 observed 17.9% NF54 plastid genotypes in NF54 x NHP4026 and 41.7% MKK2835 plastid
215 genotypes in MKK2835 x NHP1337.

216

217 **Genetic maps and recombination rates**

218 For each genetic cross, we generated a genetic map (S3 and S4 Tables) using JoinMap
219 v4.1 from phased genotype data for all unique recombinant progeny (see Methods). The map size
220 for both crosses is consistent with map lengths reported for previous crosses (1521 cM for NF54
221 x NHP4026 and 1453 cM for MKK2835 x NHP1337, Table 1). The recombination rate was 13.7
222 kb/cM for NF54 x NHP4026 and 13.8 kb/cM for MKK2835 x NHP1337, which were
223 comparable to the range observed in previous crosses (Table 1). In NF54 x NHP4026 genetic
224 map, markers initially sorted into 13 linkage groups, with each representing markers known to
225 reside on single chromosomes, with the exception of one linkage group which contained all
226 markers on chromosome 7 and 14. Adjusting joinMap parameters resulted in separating the 13th
227 linkage group into 2, recovering distinct sets for chromosomes 7 and 14. In MKK2835 x
228 NHP1337 all markers coalesced into 14 linkage groups which exactly corresponded to
229 chromosomes.

230

231 Table 1

Cross	F ₁ Progeny Number	Genetic Map Length	Recombination Rate
HB3 x Dd2	35 ^[16]	1556 ^[16]	12.1 kb/cM ^[16]
3D7 x HB3	15 ^[21]		11 kb/cM ^[30]
7G8 x GB4	32 ^[17]	1655 ^[17]	12.8 kb/cM ^[17]
GB4 x 803	27 ^[13]		13.3 kb/cM
NF54 x NHP4026	84	1521	13.7 kb/cM
MKK2835 x NHP1337	60	1453	13.8 kb/cM

232

233 To generate a graphic display of the physical map, 5 kb windows of the core genome
234 were phased to indicate inheritance blocks for each unique recombinant progeny (Fig 3A and
235 3B). NF54 x NHP4026 shows sections of the genome where inheritance is dominated by one
236 parental genotype or the other (Fig 3A). In contrast the physical recombination map for
237 MKK2835 x NHP1337 shows a more even inheritance pattern across the genome (Fig 3B).

238

239 **Repeatability of segregation distortion**

240 We observe regions with significant segregation distortion (chi squared test for deviation
241 from expected Mendelian ratio of 1:1, $p < 0.001$) in NF54 x NHP4026 that are consistent in both
242 replicates (Fig 3A and 4A). In contrast, we observe no significant segregation distortion in
243 MKK2835 x NHP1337 (Fig 3B). Specifically, in both replicates of NF54 x NHP4026 we
244 observe replicated significant deviations from the Mendelian expectation of 1:1 inheritance on
245 chromosomes 7, 12, 13 and 14 (Fig 3A) with a concordance correlation coefficient of 0.66
246 between allele frequencies in the two replicates across the genome. We initially observed the
247 segregation distortion in progeny from the NF54-GFP_{Luc} x NHP4026 cross replicate. The major
248 peak on chromosome 13 coincided with the insertion of the GFP cassette in to the *pf47* locus in

249 the NF54-GFP_{Luc} parasite which we hypothesized could be the reason for the distortion.
250 Therefore, we repeated the NF54^{WT} x NHP4026 cross using the unedited parental NF54 with
251 NHP4026 to test if the genetic modification was the driver of the distortion. This was not the
252 case and the repeatability of the skews strongly supports the alternative hypothesis that the GFP
253 cassette is not the driver of this distortion, allowing us to combine the progeny from NF54 x
254 NHP4026 in estimating genetic maps.

255

256 **Distorted Loci**

257 We examined each distorted locus for plausible driver genes.
258 Chr7: a region of 520 kb on chromosome 7 containing 121 genes showed significant segregation
259 distortion in both biological replicates of NF54 x NHP4026 (chi squared test, $p < 0.001$, Fig 4B,
260 S5 Table). This region is disproportionately inherited from NF54 with the most highly distorted
261 region having only 0.05% NHP4026 alleles in NF54GFP_{Luc} x NHP4026 replicate and 0%
262 NHP4026 in the NF54 x NHP4026 replicate. This highly distorted region contains 17 genes (Fig
263 4B) including *pfcr* (*PF3D7_0709000*). NHP4026, along with three recombinant progeny, are
264 each highly resistant to chloroquine *in vitro*. Mutations in *pfcr* are the main driver of
265 chloroquine resistance and have been shown to confer a fitness costs in some genetic
266 backgrounds [31].
267 Chr12: a 295 kb region (with 71 genes) shows replicated significant segregation distortion with
268 an overabundance of NHP4026 alleles. The most skewed region contains five genes (Fig 4C)
269 including *pfmrp2* (*PF3D7_1229100*) at the center of the peak. *Pfmrp2* has high genetic
270 variability among Thai clinical isolates with single genetic variants having significant

271 associations with *in vitro* response to chloroquine, mefloquine and piperazine and *in vivo*
272 parasite clearance [32].

273 Chr13: a 230 kb region predominantly inherited from NHP4026 with 56 genes that shows
274 replicated significant segregation distortion. The most highly distorted subregion on
275 chromosome 13 contains *pf47* (*PF3D7_1346800*). In the NF54GFPLuc x NHP4026 replicate of
276 this cross the NF54 line contained a GFPLuc cassette inserted in *pf47* [23] however this insert is
277 not present in the NF54 parent used in the NF54WT x NHP4026 replicate of this cross, which
278 shows the same distortion pattern.

279 Chr14: a 205 kb region containing 62 genes on chromosome 14 showed replicated significant
280 segregation distortion with alleles predominantly inherited from NF54. The most highly skewed
281 sub-region contains 15 genes including *pfarps10* (*PF3D7_1460900*) and has been associated
282 with slow clearance in GWAS studies [7] and is hypothesized to contribute to a permissive
283 background for evolution of *pfk13* mutations.

284 Previous *P. falciparum* genetic crosses exhibited significant segregation distortion at
285 several loci [13, 16, 17, 25]. We explored overlap between distorted regions in all the published
286 *P. falciparum* crosses and our two new crosses and included a previously published bulk analysis
287 of selection in uncloned progeny of the MKK2835xNHP1337 cross [33] (S2 Fig). We observe
288 overlaps on chromosomes 12, 13 and 14.

289

290 **Increased mapping power in an expanded genetic cross**

291 Previous genetic crosses have been used to map the genetic basis of a wide range of
292 traits. However, small sample size (Table 1) and rampant segregation distortion (S2 Fig) have
293 likely limited detection to mutations with very large effect size (ES). A quantitative dissection of

294 this has not been performed for malaria parasite crosses. To quantify the extent to which our
295 expanded progeny set will improve genetic mapping for the malaria community we performed
296 extensive simulations. We quantified the impact of phenotypic replication, progeny number and
297 the number of loci determining a trait to the power to map a trait and mapping resolution using
298 the 84 progeny from NF54 x NHP4026 (Fig 5 and S3 Fig). Briefly, we used the full progeny
299 panel from NF54 x NHP4026 ($n = 84$) or subsamples of this panel ($n = 60, 50, 40, 30$) and
300 simulated phenotypes at different effect sizes using loci with balanced inheritance (0.5 allele
301 frequency) to simulate the phenotype (see Methods for details). We then determined whether the
302 phenotype mapped to the correct loci with a significant LOD score (true positive), did not have a
303 significant association (false negative) or mapped to a different locus (false positive). Using
304 progeny panels comparable to previous genetic crosses ($n = 30-40$) only very large effect sizes
305 ($ES > 0.5$) can be mapped with high power ($>80\%$). In contrast, 84 progeny enable mapping of
306 much smaller effect sizes ($ES = 0.2$) at 80% power. Increasing the number of progeny also
307 increases the locus resolution (S3 Fig). At an ES of 0.5, with $n = 30$ we can on average map to a
308 region containing 58 genes; moreover, with $n = 84$, we can map to a region containing only 17
309 genes (S3 Fig). At small effect sizes we observe similar large increases in mapping resolution as
310 we increase the size of the progeny set and more modest increases for larger effect sizes (S3 Fig).

311 Most genetic traits are not monogenic but are complex in nature. To better capture the
312 complex genetic architecture, multiple loci must be identified and these loci sometimes interact
313 (i.e. do not contribute individually and additively). For a trait controlled by two additive loci that
314 contribute equally to the phenotype, 60 progeny, with replicated phenotypes can detect an
315 association at $ES = 0.3$, whereas 84 progeny are needed to detect an association at $ES = 0.2$.
316 When a trait is controlled by two epistatically interacting loci, 84 progeny with replicated

317 phenotypes provide 75% power to detect an association and interaction with $ES = 0.4$. Replicated
318 phenotypes allow the same power to be achieved with fewer progeny for $ES \geq 0.3$ and allow for
319 a trait with $ES = 0.2$ to be detected for $N = 84$ progeny for additive loci. This analysis indicates
320 that the four previous *P. falciparum* crosses (conducted in chimpanzee hosts) generating from 15
321 - 35 progeny, were underpowered. In progeny sets of this size could reliably detect associations
322 only for phenotypes with large effects sizes, $ES \geq 0.5$ and were not able to detect even a very
323 strong epistatic interaction. Our two new crosses with $n = 60$ and 84 progeny have much higher
324 power and are capable of reliably detecting phenotypes with effect sizes as low as 0.2.

325 Polygenic traits don't always have equal contributions from multiple loci. In malaria
326 parasites, there are several well-known phenotypes with one known major effect locus [34],
327 including chloroquine resistance and mutations in *pfcr1*, sulfadoxine and point mutations in
328 *pfdhps*, pyrimethamine and point mutations in *pfdhfr*, atovaquone and point mutation in *pfcytb*,
329 mefloquine and *pfmdr1* and artemisinin resistance and mutations in *pfk13*. It is an open question
330 whether we could detect more subtle secondary loci with genetic crosses with additional
331 progeny. Our analysis (Fig 6) shows that with 84 progeny we can detect secondary loci with ES
332 as low as 0.2 and 0.15. However, with smaller numbers of progeny we are not able to detect both
333 contributing loci. With 60 progeny we can detect only one of the secondary loci at $ES=0.2$ and
334 with 35 progeny we can detect neither secondary loci.

335

336 **Segregation distortion decreases the resolution and power of mapping**

337 Segregation distortion is abundant across nearly all *P. falciparum* genetic crosses
338 generated to date, with our newly generated MKK2835 x NHP1337 cross being the sole
339 exception. We performed a power analysis to determine the impact of segregation distortion on

340 the power to identify causal variants. Segregation distortion decreases power to detect effects
341 near the distorted locus, especially for phenotypes with small effect sizes (Fig 7). For phenotypes
342 with large effect sizes and for large numbers of progeny, the extent of segregation distortion in
343 the F₁ mapping population at the controlling locus has little effect on power; however, as the
344 number of progeny decrease, a significant loss of power occurs as the degree of segregation
345 distortion increases. The loss of power due to segregation distortion is even more pronounced
346 with fewer progeny (Fig 7). For an ES of 0.8, we can detect associations for loci with any allele
347 frequency using as little as 30 progeny. For an effect size of 0.4, 50 progeny are necessary to
348 detect an association for allele frequencies ranging from 0.3 to 0.7, and only 84 progeny will
349 allow us to detect an association at a more distorted loci with 0.2 or 0.8 allele frequency. At 0.2
350 effect size we can only reliably detect an association for a locus with even segregation using 84
351 progeny.

352 In NF54 x NHP4026 we observe significant segregation distortion ($p < 0.001$) with allele
353 frequencies at distorted loci ranging from 0.05 to 0.31 and 0.69 to 0.85 (Fig 3), including in
354 regions that include important drug resistance genes including *pfcr1* (Chromosome 7) and *pfk13*.
355 Despite this extreme segregation distortion on chromosome 7 in NF54 x NHP4026 (NHP4026
356 allele frequency of 0.05), it is still possible to map the chloroquine drug response to the locus
357 containing *pfcr1* ($p < 0.00001$, Fig 7B). In contrast, in MKK2835 x NHP1337, allele frequencies
358 of the NHP1337 alleles range from 0.3 to 0.7 (Fig 3). At these allele frequencies we see
359 consistent power indicating that power and mapping resolution are expected to be consistent
360 across the genome.

361

362 Discussion

363 **Power of *P. falciparum* genetic crosses generated using FRG NOD huHep/huRBC mice**

364 Historical challenges to generating novel *P. falciparum* genetic crosses made GWAS, *in vitro*
365 selection experiments and bulk sequencing approaches the more effective means to study new
366 drug resistance-associated phenotypes as they emerge in the clinic. However, each of these
367 techniques has its limitations. *In vitro* selections are time consuming, sometimes requiring
368 several years to produce resistant lines, and may not identify loci evolving under drug pressure in
369 the field situation [35]. GWAS is often confounded by population structure and has low power to
370 dissect complex genetic traits, i.e. multiple loci, multiple alleles per locus and epistasis [36]. On
371 the other hand, a well-conceived and controlled genetic cross can greatly complement these
372 techniques, as each cross can be designed to answer specific questions and then have high power
373 to dissect complex associations between genotype and phenotype. Historically, *P. falciparum*
374 controlled genetic crosses have been made with splenectomized chimpanzees strictly limiting
375 their production due to cost and ethical concerns. Use of the human tissue-chimeric FRG NOD
376 huHep/huRBC mouse restores and expands our ability to make controlled genetic crosses in
377 malaria parasites [23]. We demonstrate here that targeted crosses between clinical isolates can be
378 generated in real time (six months) and outperform all previous crosses in their size, mapping
379 power and precision.

380 We created the first *P. falciparum* cross between two sympatric recent clinical isolates from
381 the Thai-Myanmar border, MKK2835 and NHP1337. Analysis of the recombination rate,
382 segregation distortion, and selfing rate of this cross revealed interesting differences to all other *P.*
383 *falciparum* crosses including our NF54 x NHP4026 cross, between a lab line and a recent field
384 isolate. In MKK2835 x NHP1337 we observed minimal segregation distortion and a high
385 percentage of clones that resulted from selfing. We have also shown that most of the

386 recombinant progeny recovered are unique when cloning is initiated immediately, or within five
387 days of establishing *in vitro* culture. Using simulations, we have shown that the power to detect
388 associations between phenotypes and genotypes increases drastically when we are able to map
389 with populations with 60 – 84 individuals. We have also shown through simulation and using
390 real phenotype data that segregation distortion can lower power to detect QTL at distorted loci
391 even for phenotypes with moderate effect sizes. Nevertheless, major effect loci can be mapped
392 within these regions, supporting the utility of our crosses in these cases. Furthermore, because
393 we can cryopreserve uncloned F₁ parasite populations, it is possible to further isolate additional
394 independent recombinant progeny for future analyses, as sequential cloning attempts will isolate
395 new unique progeny.

396

397 **Power of malaria crosses generated using humanized mice**

398 We have shown that the FRG NOD huHep/huRBC mouse can be used to rapidly make
399 controlled genetic crosses on demand from field isolates to create F1 progeny populations with
400 large numbers of clonal recombinant progeny per cross. This dramatically increases our power to
401 detect associations with greater resolution. Using new crosses with more recombinant progeny
402 and higher power we can dissect genetic architecture and determine the individual contributions
403 of different loci to polygenic traits. We can also map phenotypes with small to modest effect
404 sizes more precisely, to smaller regions of the genome. For instance, at an ES of 0.5 using 30
405 recombinant progeny, we can map to a region containing 58 candidate genes. However, at an ES
406 of 0.5 using 84 progeny, we can map to a region of 17 candidate genes (S3 Fig). With increased
407 transfection efficiencies using CRISPR/Cas9-based technology, it is not unreasonable to then
408 target the genome by transgenesis to pinpoint loci involved in observed phenotypes. For

409 phenotypes with large ES, similar to that conferred by chloroquine resistance (0.8), with 30
410 progeny we can map to a region containing on average 20 candidate genes whereas with 84
411 progeny we can map to a region containing only eight genes. These significant reductions in
412 number of candidate genes has a large impact on our ability to determine causal mutations,
413 drastically reducing the effort required for validation studies. Furthermore, our ability to generate
414 further genetic crosses between the same two parents of interest is unparalleled, allowing us to
415 potentially isolate 100's of unique recombinant progeny for analysis.

416

417 **Maximizing Numbers of Unique Recombinant Progeny**

418 Based on the prevalence of infected mosquitos and estimates of oocysts/mosquito we can
419 estimate the number of unique recombinants in the mosquitos used to infect each FRG NOD
420 huHep/huRBC mouse. During the parasite lifecycle there are multiple bottlenecks which reduce
421 the number of genotypes in a blood stream infection. Oocysts may arise due to selfing or fail to
422 progress, sporozoites may fail to reach the liver and further attrition through the liver and blood
423 stages will occur. As we observed, without extensive cloning efforts we are unable to capture all
424 these possible unique recombinant progeny. Interestingly, each cloning round produced almost
425 entirely unique sets of progeny indicating that our cloning efforts (166 clones for NF54 x
426 NHP4026 and 266 for MKK2835 x NHP1337) under-sampled the total population of
427 recombinant progeny available. Recovering unique sets of progeny from each cloning round
428 indicates that there are likely many more additional unique progeny to recover from the bulk F_1
429 populations and that strategic additional cloning would likely provide a substantial return in F_1
430 progeny numbers. In order to maximize the number of unique recombinant progeny recovered,
431 we showed that cloning straight after the *in vivo* liver stage to blood stage transition or as early as

432 possible after establishing *in vitro* culture gave a large degree of success. Also, initiating cloning
433 either directly from the mouse or from a thawed stock of bulk culture did not impact the
434 proportion of unique recombinant progeny recovered. Notably, we minimized the potential for
435 additional loss in diversity during cryopreservation by freezing immediately after exsanguination
436 and cloning within 48 hours of thaw. Additionally, with streamlining of the crossing process and
437 being able to complete a cross from thawing of parental lines to isolating, genotyping and
438 identifying unique recombinant progeny within 6 months it is easy to simply repeat the cross and
439 generate an entirely distinct set of recombinant progeny to generate additional unique
440 recombinant progeny.

441

442 **Differences in selfing between crosses**

443 *P. falciparum* infections in nature are sometimes monoclonal and sometimes co-infections,
444 depending on the genetic diversity of the gametocytes taken up during a mosquito blood meal.
445 Thus, *P. falciparum* must be able to maintain its life-cycle through selfing as well as out-
446 crossing. Evidence from natural infections suggests that mating can be non-random when
447 distinct parasite lineages are co-transmitted from a single mosquito bite [37]. In previous crosses
448 between established lab lines 3D7 and HB3, it was shown that selfed progeny are observed at
449 expected ratios in oocysts [38, 39] and early in blood stage culture, but at lower than expected
450 ratios among clones when cloning was begun 32 days after isolation from chimpanzees [40, 41].
451 In 7G8 x GB4, 29 of more than 200 (14.5%) individual clones were selfed [25].

452 Our MKK2835 x NHP1337 cross between two recent field isolates, both from Southeast
453 Asia, produced more selfed progeny than previously reported for *P. falciparum* genetic crosses.
454 Interestingly, NHP1337 dominated the selfed progeny almost entirely, consistent with bulk allele

455 frequencies in samples taken at similar times [33]. While efforts were made to infect the
456 mosquitos with equal number of MKK2835 x NHP1337 gametocytes, the unequal selfing rates
457 may reflect an imbalance in the initial gametocyte ratio or in gametocyte viability between
458 MKK2835 and NHP1337. It is also possible that there are inherent difference in selfing rates
459 between MKK2835 and NHP1337, although both lines successfully selfed in mosquito cages
460 infected with only one parent (S1 Table). We do not yet know if the large proportion of selfed
461 clones observed in our cross between recent field isolates will be repeated in future crosses.
462 Using bulk segregant analysis of these same populations we suspect that these selfed clones are
463 outcompeted over time in non-stressed *in vitro* culture conditions [33] this may perhaps also
464 have been the case in the previous 3D7 x HB3 cross [39, 40].

465 In contrast we observed very few selfed progeny in our NF54 x NHP4026 cross, between a
466 recent Southeast Asian field isolate NHP4026 and the established African lab line NF54. Both
467 NF54 and NHP4026 readily self when in used alone to inoculate mosquito cages with NF54
468 often giving very high infection prevalence and numbers of oocysts/midgut (S1 Table). In
469 several cloning rounds of NF54 x NHP4026, cloning was initiated immediately after transition to
470 *in vitro* culture, indicating that in this cross selfed progeny were not selected against in bulk
471 competition with recombinant progeny. Further experiments will be necessary to understand why
472 NF54 x NHP4026 generated so few selfed progeny.

473

474 **Differences in segregation distortion between crosses**

475 In other systems segregation distortion is often more extreme when more distantly related
476 parents are crossed. For instance, interspecific crosses have been shown to result in segregation
477 distortion more often and with more severe distortion than intraspecific crosses [42, 43]. All

478 previous *P. falciparum* genetic crosses were between allopatric parasite lines, generally isolated
479 on different continents, and unsurprisingly show significant segregation distortion over large
480 regions of the genome. Similar to previous *P. falciparum* crosses, our allopatric cross between an
481 establish lab line (NF54 or NF54GFPLuc, African origin) and a recent field isolate (NHP4026,
482 Thai-Myanmar border) had regions of significant segregation distortion that were consistent
483 across replicates. Conversely, the MKK2835 x NHP1337 cross which relied on two sympatric
484 parasites recently isolated from the Thai-Myanmar border was the first *P. falciparum* controlled
485 genetic cross to have relatively even inheritance patterns across the genome with no significant
486 segregation distortion. One possible explanation for the observed segregation distortion is that
487 natural selection may act against unfit allele combinations causing a deviation from expected
488 mendelian ratios [44]. It is also possible that there are prezygotic barriers such as barriers to
489 gamete recognition between more distantly related parents.

490 In NF54 x NHP4026, the subregions with the most highly skewed allele frequencies in each
491 of the significantly distorted regions contain genes of interest. The most highly distorted
492 subregion on chromosome 7 (predominantly inherited from the NF54 parent with only 3 progeny
493 inheriting alleles from NHP4026) includes *pfCRT* which is known to carry a substantial fitness
494 cost in some genetic backgrounds and that different combinations of mutations are more
495 deleterious than others [31]. Although NHP4026 is a parasite that grows particularly well in *in*
496 *vitro* culture [45] (even outcompeting NF54 in co-culture experiments) it is clear that inheriting
497 an NHP4026 allele at this locus contributes a fitness cost. The most highly skewed subregion on
498 chromosome 14 is also predominantly inherited from NF54 and contains *pfPRP2* which has been
499 associated with artemisinin resistance (slow clearance of parasite from treated patients) in
500 GWAS studies and is thought to contribute to a permission background for development of

501 artemisinin resistance [7]. While NHP4026 is *pfk13* WT it does have a slow clearance
502 phenotype. It will be interesting to explore whether *pfarps10* has a fitness cost in this genetic
503 background. Interestingly, while we see no segregation distortion in MKK2835 x NHP1337
504 among the cloned progeny, we do see selection on chromosome 14 over time in a uncloned bulk
505 culture of MKK2835 x NHP1337 cross F₁ progeny that is also centered on *pfarps10* where
506 selection is against the derived alleles in *pfarps10* [33].

507 Alternatively, on chromosomes 12 and 13 there are subregions where alleles are more
508 commonly inherited from NHP4026. The region on chromosome 12 include *pfmrp2* and the
509 region on chromosome 13 includes *pf47*. The most skewed region on chromosome 12 overlaps
510 with the selected region in a uncloned bulk culture of MKK2835 x NHP1337 cross F₁ progeny
511 except that selection is against the derived allele in *pfmrp2* in this case. *Pfmrp2* has been
512 associated with mefloquine and piperazine response *in vitro* and parasite clearance [32] in Thai
513 isolates and we speculate it may have a fitness cost *in vitro*. The role *pfmrp2* plays in drug
514 resistance is still unclear and these genetic crosses may help elucidate its function. In the
515 NF54GFPLux x NHP4026 replicate, the NF54 parent contained a *gfp/luciferase* cassette insert
516 on chromosome 13 in *pf47*, the NF54WT x NHP4026 replicate of this cross was made with the
517 isogenic NF54 line without the *gfp/luciferase* insert. We saw consistent inheritance patterns in
518 both biological replicates of this cross indicating the skew here is *gfp/luciferase* insert
519 independent. A large region of segregation distortion was observed on chromosome 13 in 7G8 x
520 GB4, part of which overlaps our region of segregation distortion in NF54 x NHP4026 [17, 25].
521 *Pf47* and *pfs45/48*, two 6-cys proteins are located in the center of this subregion. These two
522 genes are known to be highly polymorphic in natural populations and are thought to be under
523 selection because of roles in gamete recognition and compatibility [46, 47]. It is possible that

524 *pf47* and/or *pfs45/48* play a key role in segregation distortion in more distantly related lines but
525 not in a cross between allopatric recent clinical isolates. Indeed, we observed no significant
526 segregation distortion in the MKK2835 cross and also observed no selection over time on
527 chromosome 13 in the bulk segregant experiment using the MKK2835 x NHP1337 bulk F₁
528 progeny [33].

529 We think that natural selection acting against unfit allele combinations is a plausible
530 explanation for some regions of segregation distortion in NF54 x NHP4026 including the regions
531 on chromosome 7, 12 and 14 and the observed selection over time in the uncloned bulk F₁
532 culture from the MKK2835 x NHP1337 cross [33]. Issues with gamete recognition and
533 compatibility might drive segregation distortion observed on chromosome 13 in NF54 x
534 NHP4026 and 7G8 x GB4 (both allopatric) but not in the sympatric MKK2835 x NHP1337 cross
535 (see also [33]). Performing competition experiments between individual progeny with different
536 alleles at these distorted and selected loci will be informative in determining how different
537 combinations of alleles might contribute to parasite fitness [45]. These experiments can be
538 followed with CRISPR/Cas9 editing of polymorphisms in individual genes as further validation.

539

540 **Loss of power at segregation distortion loci**

541 Segregation distortion loci traditionally have been excluded in genetic mapping studies to
542 avoid loss of power to detect real effects (type II error, false negative) and the potential to detect
543 false positives (type I error) [48]. Excluding distorted loci from analysis would be particularly
544 problematic in *P. falciparum* because all previous crosses had large regions of significant
545 segregation distortion that contain known resistance loci. Using segregation distortion loci in
546 mapping studies is possible, however it is necessary to carefully interpret results keeping in mind

547 the loss of power to detect effects in distorted regions. If drug resistance loci are at or near
548 genome regions showing segregation distortion loci, we may fail to detect these drug resistance
549 loci in crosses with small numbers of progeny or when effect size is small. We have shown this
550 effect through mapping simulated phenotypes to loci with varying degrees of segregation
551 distortion. Despite the extreme segregation distortion observed in NF54 x NHP4026 (NHP4026
552 allele frequency of less than 0.05 at *pfprt*) and only three progeny plus NHP4026 showing a
553 chloroquine resistant phenotype we are able to correctly map the chloroquine drug response to
554 the locus containing *pfprt*. Through simulation, we demonstrate reliable detection of QTL for
555 phenotypes with very large effect sizes (ES = 0.8), even for very distorted loci and small
556 numbers of progeny. However, as the effect size decreases, we observe stronger loss of power at
557 distorted loci. For phenotypes with moderate effect sizes we can only reliably detect QTL at
558 distorted loci using large numbers of progeny. Therefore, care is required in interpreting negative
559 QTL results for phenotypes with small to moderate effect sizes, especially when mapping in
560 small progeny sets. When QTL and segregation distortion loci coincide, false negatives will lead
561 us to miss real associations between phenotypes and genetic variants. This problem with power
562 will be amplified when attempting to map omics phenotypes where multiple testing correction
563 must be employed. However, while segregation distortion presents a challenge for linkage
564 analysis, the location of genome regions showing strong skews can help to pinpoint loci with
565 large phenotypic effects.

566

567 **Conclusions**

568 We believe that the use of the human hepatocyte-chimeric FRG NOD huHep/huRBC
569 mouse to generate genetic crosses in *P. falciparum* has the potential to revolutionize quantitative

570 genetics in *P. falciparum*. It is feasible to generate crosses on demand to study the genetic
571 architecture of emerging phenotypes. We can also use complex cross designs to improve power
572 to detect associations for phenotypes where a genetic variant only controls a small amount of
573 variation. Shared parent crosses are ideal for understanding the role of individual mutations
574 within phenotypes with complex genetic architecture. Pairwise crosses of a small group of
575 isolates can be used to create a diversity panel that captures a large amount of phenotypic and
576 genetic variation in *P. falciparum*. Similarly, many other complex cross designs that have been
577 used extensively in the plant and animal breeding literature that are now open to malaria
578 researchers.

579

580 **Methods**

581 Genetic crosses were conducted largely as described previously [23]. We made several
582 adjustments to maximize recovery of progeny from the genetic crosses, including completing
583 independent replicates of the crosses and cloning via limiting dilution directly from the
584 transitioned blood removed from the FRG NOD huHep mouse. In addition, the transition to *in*
585 *vitro* culture was carried out using media containing Albumax rather than human serum. We
586 observed successful expansion of the transitioned cultures in both serum-containing and
587 Albumax-containing media, but downstream limiting dilution cloning failed to yield the expected
588 number of clones if carried out using serum. We therefore cloned and expanded the transitioned
589 blood stage culture in media containing Albumax. Screening for clones was carried out using the
590 Phusion Blood Direct PCR Kit (Thermo Scientific). Specific methodological information for
591 each replicate of each cross is provided in S2 Table.

592

593 **Identifying Positive Clones**

594 Beginning at week 2 post cloning and continuing until week 6 the Phusion Blood Direct
595 PCR Kit (Thermo Scientific) was utilized to identify positive clones. This kit is very sensitive,
596 detecting positive parasitemia using only 1 μ L of infected culture streamlining our detection of
597 positive clones. A protocol for this screening method is available in the S1 File.

598

599 **MS Genotyping**

600 All progeny of NF54 x NHP4026 were initially genotyped via microsatellite markers to
601 identify unique recombinants. The progeny isolated in cloning rounds 1 and 2 or replicate 1 of
602 the NF54 x NHP4026 were genotyped at 17 MS markers. The progeny isolated in cloning round
603 3 of NF54 x NHP4026 were genotyped at 8 MS markers. Primers for each MS marker used are
604 listed in S6 Table. For cloning rounds 1 and 2, full genome sequencing was performed for all
605 unique recombinants. For cloning round 3 and all other crosses all potential recombinant progeny
606 were fully sequenced.

607

608 **Preparation and sequencing of progeny**

609 DNA was extracted from 35-50 μ L of packed red blood cells using Quick DNA Kit (Zymo).
610 Libraries were prepared with $\frac{1}{4}$ reaction volumes of the KAPA HyperPlus DNA Library Kit and
611 20-50ng of extracted DNA according to manufacturer directions with slight modifications.
612 Fragmentation time was 26 minutes; adapter ligation was increased to 1 hour; PCR was
613 performed for 7 cycles; and size selection was performed post PCR using full volume methods.
614 We used KAPA Dual-Indexed Adapter Kit, adding 7.5 μ M adapter to the appropriate well.
615 Samples were measured for DNA quantity using the QBit BR DNA Kit. Samples were then

616 pooled for sequencing based on their QBit measurements to normalize input. The pooled sample
617 was quantified using the KAPA Library Quantification Kit, and adjusted to 2-4nM with 10mM
618 Tris-HCl, pH 7.5-8.0 (Qiagen) for sequencing on Illumina platforms. The pool was also run on
619 the Agilent Tape Station using the D1000 BR Kit to assess sample size and lack of primer
620 dimers. Pools were run on the Illumina HiSeq 2500 or Illumina NextSeq for 2x100bp run
621
622 We aligned raw sequencing reads to v3 of the 3D7 genome reference (<http://www.plasmodb.org>)
623 using BWA MEM v0.7.5a [49]. After removing PCR duplicates and reads mapping to the ends
624 of chromosomes (Picard v1.56) we recalibrated base quality scores, realigned around indels and
625 called genotypes using GATK v3.5 [50] in the GenotypeGVCFs mode using QualByDepth,
626 FisherStrand, StrandOddsRatio VariantType, GC Content and max_alterate_alleles set to 6. We
627 recalibrated quality scores and calculated VQSLOD scores using SNP calls conforming to
628 Mendelian inheritance in previous genetic crosses, and excluding sites in highly error-prone
629 genomic regions (calls outside of the “core genome” [21]).

630

631

632 **Filtering high quality SNP variants**

633 The .vcf file containing parents, potential progeny and all high quality SNPs were
634 processed in R using the vcfR library. Initially SNP filters were based on the parental
635 distributions; only homozygous, bi-allelic parental SNPs with high coverage (≥ 10) and high
636 quality scores ($GQ \geq 99$) were retained. Next, low quality SNPs across parents and progeny were
637 filtered with a $VQSLOD < 2.5$. This final SNP set was defined as our high quality SNP set for
638 further analysis.

639

640 **Filtering Progeny**

641 In *P. falciparum* crosses to produce the F₁ mapping population, it is necessary to filter out
642 potential progeny that are non-clonal and repeated sampling of the same genotype. Initially,
643 potential progeny with more than 80% missing data were removed from further analysis.

644

645 **Identifying and filtering non-clonal progeny**

646 Since *P. falciparum* parasites are haploid throughout the entirety of the human portion of
647 their life-cycle including the intraerythrocytic stage during which they are cloned we expect that
648 clonal infections should have predominantly homozygous SNP calls except for rare instances of
649 sequencing error. In contrast, non-clonal infections where the mixture contains full siblings or
650 full siblings and parent genotypes would have contiguous regions with high numbers of
651 heterozygous SNP calls at above the rate expected from sequencing error along.

652 The sequencing error rate was estimated for each cross as the mean from a distribution of
653 percent heterozygous SNP calls across all potential progeny (S4 Fig). Assuming true sequencing
654 errors follow a Poisson process with $\lambda = \%$ sequencing error, then the expected distance between
655 sequencing events as $1/\lambda$. To identify non-clonal samples we counted heterozygous SNP calls
656 across the genome in a sliding window of size $1/\lambda$ and using a Poisson Distribution with $\lambda = \%$
657 sequencing error calculated the probability of getting at least the observed number of
658 heterozygous SNP calls in each window. These probabilities were adjusted for multiple testing
659 based on the number of windows in the genome and the adjusted probabilities were plotted as a
660 heatmap (S4 Fig). Samples with windows with adjusted probabilities < 0.05 were designated as
661 non-clonal and filtered from the final progeny set.

662

663 **Phasing of clonal progeny**

664 A matrix of phased genotypes was constructed for parents and clonal progeny for all high
665 quality SNPs. In each cross the drug sensitive parents (NF54 and MKK2835) were coded as 0
666 while the drug resistant parent (NHP4026 and NHP1337) were coded as 1. Progeny SNPs that
667 matched the drug sensitive parent's SNPs were coded as 0 while SNPs that matched the drug
668 resistant parent's SNPs were coded as 1. Heterozygous SNPs were coded as missing.

669

670 **Identifying Unique Recombinants**

671 Our high quality phased dataset for clonal progeny was formatted for the qtl package in R
672 and loaded as a genetic map. Genotype similarity scores were computed using the comparegeno
673 function. A similarity score cut-off of 0.9 was used to define clusters of genetically distinct
674 recombinant progeny (see S1 File for details of cut-off was chosen). Individual progeny were
675 selected from each cluster of genetically similar progeny using igraph in R. Only unique
676 recombinant progeny and parents were retained to create a final dataset of all SNPs.

677

678 **Physical Recombination Map Construction**

679 5kb windows were defined across the core genome to construct a heatmap depicting a
680 physical recombination map for each cross. For each progeny, in each 5kb window the most
681 common parental genotype was determined, if a window contained only missing data then it was
682 filled if the next window with data had a matching genotype to the previous window with data,
683 otherwise it was left missing.

684

685 **Defining informative markers**

686 All phased genotype data for clonal, unique recombinant progeny and parents were
687 loaded into R qtl as a genetic map. The findDupMarkers function was used to identify clusters of
688 markers with identical genotype data and the central marker from each cluster was retained in a
689 set of informative markers. This set of informative genotype markers for all clonal, unique
690 recombinant progeny was used for all subsequent analysis and figures. The entire filtering
691 pipeline is available on github (<https://github.com/MalariaMCG/CrossProgenyCharacterization>)
692 with documentation.

693

694 **Genetic Map Construction**

695 For each cross the set of informative genotype markers for clonal unique recombinant
696 progeny was coded as A for the sensitive parent and B for the resistant parent and – for missing
697 data and loaded into JoinMapv4.1. Population type was set to HAP1 and the Kosambi mapping
698 function was employed in generating each genetic map. All other parameters were initially set to
699 defaults, however, to account for the systemic segregation distortion observed in the
700 NF54xNHP4026 cross it was necessary to expand the population threshold ranges such that the
701 independence LOD ranged from 1.0 to 15.0, the independence P-value from 1.0e-3 to 1.0e-5, the
702 recombination frequency from 0.250 to 0.001 and the linkage LOD from 3.0 to 15.0. This change
703 in parameters allowed us to differentiate between SNP markers with similar distortion patterns
704 that were known to be physically located on different chromosomes.

705

706 **Power Analysis**

707 Progeny from NF54 x NHP4026 were used to estimate power under three different
708 scenarios, one genetic locus contributing to phenotypic variation, 2 loci with additive
709 contributions to phenotypic variation and 2 loci with epistatic interaction controlling phenotypic
710 variation. All models were simulated for the full F₁ progeny set with N=84 and for subsamples
711 with N=30, 40, 50, 60 and 70. Under the one locus model, a phenotype was simulated as either a
712 single replicate value or the average of 5 replicates at effect sizes ranging from 0.1 to 0.8. Under
713 the two additive loci model, a phenotype was simulated as either a single replicate value or the
714 average of 5 replicates for effect sizes for each locus ranging from 0.1 to 0.4. Under the two
715 epistatic loci model, the first locus controlled whether a trait was present in an on/off fashion and
716 the second locus controlled the level of the phenotype (ie. locus 1 is necessary to be drug
717 resistant and locus 2 controls the level of resistance) and the main effects of both loci ranged
718 between 0.1 to 0.4. A set of markers with 1:1 mendelian inheritance patterns were used as the 1
719 or 2 loci in the models. All qtl mapping was performed with r qtl. For each simulation,
720 significance thresholds were defined based on 1000 permutations. True positives were defined as
721 a LOD peak that meant the $\alpha=0.05$ significance threshold and whose 1.5 LOD interval contained
722 the actual marker used in the model.

723

724 **SD Power Analysis**

725 This analysis was similar to the 1 locus model in the previous section. In these
726 simulations effect sizes were calculated based on balanced inheritance and levels included 0.2,
727 0.3, 0.4, 0.6 and 0.8. All markers were categorized by their allele frequency and sorted into bins
728 for each level of allele frequency skew (ie. 0.89 to 0.91 and 0.09 to 0.11 were in the 0.1 bin

729 which represented the most skewed alleles in this analysis). QTL mapping, significance levels
730 and definition of true positives were that same as in the power analysis above.

731

732 **Acknowledgements**

733 We would like to thank Jasmine Clark for help with progeny cloning. We would like to
734 acknowledge members of the Ferdig lab, Anderson lab, Cheeseman lab, Vaughan lab, Kappe
735 labs and Emrich lab for helpful discussions.

736

737 **References**

738

- 739 1. Fairlamb AH, Gow NAR, Matthews KR, Waters AP. Drug resistance in eukaryotic
740 microorganisms. *Nature Microbiology*. 2016;1(7). doi: 10.1038/nmicrobiol.2016.92.
- 741 2. Wang W, Wang L, Liang Y-S. Susceptibility or resistance of praziquantel in human
742 schistosomiasis: a review. *Parasitology Research*. 2012;111(5):1871-7. doi:
743 10.1007/s00436-012-3151-z.
- 744 3. Ferdig MT, Cooper RA, Mu J, Deng B, Joy DA, Su XZ, et al. Dissecting the loci of low-level
745 quinine resistance in malaria parasites. *Mol Microbiol*. 2004;52(4):985-97. doi:
746 10.1111/j.1365-2958.2004.04035.x".
- 747 4. Müller IB, Hyde JE. Antimalarial drugs: modes of action and mechanisms of parasite
748 resistance. *Future Microbiology*. 2010;5(12):1857-73. doi: 10.2217/fmb.10.136.

- 749 5. Chevalier FD, Valentim CLL, LoVerde PT, Anderson TJC. Efficient linkage mapping using
750 exome capture and extreme QTL in schistosome parasites. *BMC Genomics*. 2014;15(1).
751 doi: 10.1186/1471-2164-15-617.
- 752 6. Alsford SAM, Kelly JM, Baker N, Horn D. Genetic dissection of drug resistance in
753 trypanosomes. *Parasitology*. 2013;140(12):1478-91. doi: 10.1017/s003118201300022x.
- 754 7. Miotto O, Amato R, Ashley EA, MacInnis B, Almagro-Garcia J, Amaratunga C, et al. Genetic
755 architecture of artemisinin-resistant *Plasmodium falciparum*. *Nature genetics*.
756 2015;47(3):226-34.
- 757 8. Arieu F, Witkowski B, Amaratunga C, Beghain J, Langlois A-C, Khim N, et al. A molecular
758 marker of artemisinin-resistant *Plasmodium falciparum* malaria. *Nature*.
759 2014;505(7481):50-5.
- 760 9. Straimer J, Gnadig NF, Witkowski B, Amaratunga C, Duru V, Ramadani AP, et al. Drug
761 resistance. K13-propeller mutations confer artemisinin resistance in *Plasmodium*
762 *falciparum* clinical isolates. *Science (New York, NY)*. 2015;347(6220):428-31. doi:
763 10.1126/science.1260867 [doi].
- 764 10. Cheeseman IH, Miller BA, Nair S, Nkhoma S, Tan A, Tan JC, et al. A major genome region
765 underlying artemisinin resistance in malaria. *Science (New York, NY)*. 2012;336(6077):79-
766 82. doi: 10.1126/science.1215966 [doi].
- 767 11. Fidock DA, Nomura T, Talley AK, Cooper RA, Dzekunov SM, Ferdig MT, et al. Mutations in
768 the *P. falciparum* digestive vacuole transmembrane protein PfCRT and evidence for their
769 role in chloroquine resistance. *Mol Cell*. 2000;6(4):861-71. Epub 2000/11/25. PubMed
770 PMID: 11090624; PubMed Central PMCID: PMCPMC2944663.

- 771 12. Valentim CLL, Cioli D, Chevalier FD, Cao X, Taylor AB, Holloway SP, et al. Genetic and
772 Molecular Basis of Drug Resistance and Species-Specific Drug Action in Schistosome
773 Parasites. *Science*. 2013;342(6164):1385-9. doi: 10.1126/science.1243106.
- 774 13. Sá JM, Kaslow SR, Krause MA, Melendez-Muniz VA, Salzman RE, Kite WA, et al.
775 Artemisinin resistance phenotypes and K13 inheritance in a *Plasmodium falciparum* cross
776 and *Aotus* model. *Proceedings of the National Academy of Sciences*. 2018. doi:
777 10.1073/pnas.1813386115.
- 778 14. MacLeod A. The genetic map and comparative analysis with the physical map of
779 *Trypanosoma brucei*. *Nucleic Acids Research*. 2005;33(21):6688-93. doi:
780 10.1093/nar/gki980.
- 781 15. Cheeseman IH, McDew-White M, Phyto AP, Sriprawat K, Nosten F, Anderson TJ. Pooled
782 sequencing and rare variant association tests for identifying the determinants of emerging
783 drug resistance in malaria parasites. *Mol Biol Evol*. 2015;32(4):1080-90. Epub 2014/12/24.
784 doi: 10.1093/molbev/msu397. PubMed PMID: 25534029; PubMed Central PMCID:
785 PMC4379400.
- 786 16. Su X, Ferdig MT, Huang Y, Huynh CQ, Liu A, You J, et al. A genetic map and recombination
787 parameters of the human malaria parasite *Plasmodium falciparum*. *Science*.
788 1999;286(5443):1351-3. Epub 1999/11/13. PubMed PMID: 10558988.
- 789 17. Jiang H, Li N, Gopalan V, Zilversmit MM, Varma S, Nagarajan V, et al. High recombination
790 rates and hotspots in a *Plasmodium falciparum* genetic cross. *Genome Biol*.
791 2011;12(4):R33. Epub 2011/04/06. doi: 10.1186/gb-2011-12-4-r33. PubMed PMID:
792 21463505; PubMed Central PMCID: PMC3218859.

- 793 18. Gardner MJ, Hall N, Fung E, White O, Berriman M, Hyman RW, et al. Genome sequence of
794 the human malaria parasite *Plasmodium falciparum*. *Nature*. 2002;419(6906):498-511.
795 doi: 10.1038/nature01097. PubMed PMID: 12368864; PubMed Central PMCID:
796 PMC3836256.
- 797 19. Aurrecochea C, Brestelli J, Brunk BP, Dommer J, Fischer S, Gajria B, et al. PlasmoDB: a
798 functional genomic database for malaria parasites. *Nucleic acids research*.
799 2009;37(Database issue):D539-43. doi: 10.1093/nar/gkn814 [doi].
- 800 20. Aurrecochea C, Barreto A, Basenko EY, Brestelli J, Brunk BP, Cade S, et al. EuPathDB: the
801 eukaryotic pathogen genomics database resource. *Nucleic Acids Research*.
802 2017;45(D1):D581-D91. doi: 10.1093/nar/gkw1105.
- 803 21. Miles A, Iqbal Z, Vauterin P, Pearson R, Campino S, Theron M, et al. Indels, structural
804 variation, and recombination drive genomic diversity in *Plasmodium falciparum*. *Genome*
805 *Res*. 2016;26(9):1288-99. doi: 10.1101/gr.203711.115. PubMed PMID: 27531718; PubMed
806 Central PMCID: PMC5052046.
- 807 22. Flint J, Mackay TFC. Genetic architecture of quantitative traits in mice, flies, and humans.
808 *Genome Research*. 2009;19(5):723-33. doi: 10.1101/gr.086660.108.
- 809 23. Vaughan AM, Pinapati RS, Cheeseman IH, Camargo N, Fishbaugher M, Checkley LA, et al.
810 *Plasmodium falciparum* genetic crosses in a humanized mouse model. *Nature Methods*.
811 2015;12(7):631-3. doi: 10.1038/nmeth.3432.
- 812 24. Mott BT, Eastman RT, Guha R, Sherlach KS, Siriwardana A, Shinn P, et al. High-throughput
813 matrix screening identifies synergistic and antagonistic antimalarial drug combinations.
814 *Scientific reports*. 2015;5:13891. doi: 10.1038/srep13891 [doi].

- 815 25. Hayton K, Gaur D, Liu A, Takahashi J, Henschen B, Singh S, et al. Erythrocyte Binding
816 Protein PfrH5 Polymorphisms Determine Species-Specific Pathways of Plasmodium
817 falciparum Invasion. *Cell Host & Microbe*. 2008;4(1):40-51. doi:
818 10.1016/j.chom.2008.06.001.
- 819 26. Logan-Klumpler FJ, De Silva N, Boehme U, Rogers MB, Velarde G, McQuillan JA, et al.
820 GeneDB--an annotation database for pathogens. *Nucleic Acids Res*. 2012;40(Database
821 issue):D98-108. Epub 2011/11/26. doi: 10.1093/nar/gkr1032. PubMed PMID: 22116062;
822 PubMed Central PMCID: PMC3245030.
- 823 27. Okamoto N, Spurck TP, Goodman CD, McFadden GI. Apicoplast and Mitochondrion in
824 Gametocytogenesis of Plasmodium falciparum. *Eukaryotic Cell*. 2009;8(1):128-32. doi:
825 10.1128/ec.00267-08.
- 826 28. Vaidya AB, Morrissey J, Plowe CV, Kaslow DC, Wellems TE. Unidirectional dominance of
827 cytoplasmic inheritance in two genetic crosses of Plasmodium falciparum. *Molecular and*
828 *Cellular Biology*. 1993;13(12):7349-57. doi: 10.1128/mcb.13.12.7349.
- 829 29. Creasey AM, Ranford-Cartwright LC, Moore DJ, Williamson DH, Wilson RJ, Walliker D, et
830 al. Uniparental inheritance of the mitochondrial gene cytochrome b in Plasmodium
831 falciparum. *Curr Genet*. 1993;23(4):360-4. Epub 1993/01/01. doi: 10.1007/bf00310900.
832 PubMed PMID: 8467535.
- 833 30. Ranford-Cartwright LC, Mwangi JM. Analysis of malaria parasite phenotypes using
834 experimental genetic crosses of Plasmodium falciparum. *International Journal for*
835 *Parasitology*. 2012;42(6):529-34. doi: 10.1016/j.ijpara.2012.03.004. PubMed PMID:
836 WOS:000305720200003.

- 837 31. Gabryszewski SJ, Modchang C, Musset L, Chookajorn T, Fidock DA. Combinatorial Genetic
838 Modeling of pfprt-Mediated Drug Resistance Evolution in *Plasmodium falciparum*.
839 *Molecular Biology and Evolution*. 2016;33(6):1554-70. doi: 10.1093/molbev/msw037.
- 840 32. Veiga MI, Osorio NS, Ferreira PE, Franzen O, Dahlstrom S, Lum JK, et al. Complex
841 polymorphisms in the *Plasmodium falciparum* multidrug resistance protein 2 gene and its
842 contribution to antimalarial response. *Antimicrob Agents Chemother*. 2014;58(12):7390-7.
843 Epub 2014/10/01. doi: 10.1128/AAC.03337-14. PubMed PMID: 25267670; PubMed
844 Central PMCID: PMCPMC4249497.
- 845 33. Li X, Kumar S, McDew-White M, Haile M, Cheeseman IH, Emrich S, et al. Genetic mapping
846 of fitness determinants across the malaria parasite *Plasmodium falciparum* life cycle. *PLoS*
847 *Genet*. 2019;15(10):e1008453. Epub 2019/10/15. doi: 10.1371/journal.pgen.1008453.
848 PubMed PMID: 31609965; PubMed Central PMCID: PMCPMC477818.
- 849 34. Parija S, Antony H. Antimalarial drug resistance: An overview. *Tropical Parasitology*.
850 2016;6(1). doi: 10.4103/2229-5070.175081.
- 851 35. Nzila A, Mwai L. In vitro selection of *Plasmodium falciparum* drug-resistant parasite lines. *J*
852 *Antimicrob Chemother*. 2010;65(3):390-8. Epub 2009/12/22. doi: 10.1093/jac/dkp449.
853 PubMed PMID: 20022938; PubMed Central PMCID: PMCPMC2818104.
- 854 36. Morgante F, Huang W, Maltecca C, Mackay TFC. Effect of genetic architecture on the
855 prediction accuracy of quantitative traits in samples of unrelated individuals. *Heredity*.
856 2018;120(6):500-14. doi: 10.1038/s41437-017-0043-0.

- 857 37. Michel K, Morlais I, Nsango SE, Toussile W, Abate L, Annan Z, et al. Plasmodium falciparum
858 Mating Patterns and Mosquito Infectivity of Natural Isolates of Gametocytes. Plos One.
859 2015;10(4). doi: 10.1371/journal.pone.0123777.
- 860 38. Ranford-Cartwright LC. Fit for fertilization: Mating in malaria parasites. Parasitology
861 Today. 1995;11(4):154-7. doi: 10.1016/0169-4758(95)80138-3.
- 862 39. Ranford-Cartwright LC, Balfe P, Carter R, Walliker D. Frequency of cross-fertilization in the
863 human malaria parasite Plasmodium falciparum. Parasitology. 2009;107(01). doi:
864 10.1017/s003118200007935x.
- 865 40. Walliker D, Quakyi IA, Wellems TE, McCutchan TF, Szarfman A, London WT, et al. Genetic
866 analysis of the human malaria parasite Plasmodium falciparum. Science.
867 1987;236(4809):1661-6. Epub 1987/06/26. PubMed PMID: 3299700.
- 868 41. Walker-Jonah A, Dolan SA, Gwadz RW, Panton LJ, Wellems TE. An RFLP map of the
869 Plasmodium falciparum genome, recombination rates and favored linkage groups in a
870 genetic cross. Molecular and Biochemical Parasitology. 1992;51(2):313-20. doi:
871 10.1016/0166-6851(92)90081-t.
- 872 42. Myburg AA, Vogl C, Griffin AR, Sederoff RR, Whetten RW. Genetics of postzygotic isolation
873 in Eucalyptus: whole-genome analysis of barriers to introgression in a wide interspecific
874 cross of Eucalyptus grandis and E. globulus. Genetics. 2004;166(3):1405-18. Epub
875 2004/04/15. PubMed PMID: 15082559; PubMed Central PMCID: PMC1470765.
- 876 43. Yin TM, DiFazio SP, Gunter LE, Riemenschneider D, Tuskan GA. Large-scale heterospecific
877 segregation distortion in Populus revealed by a dense genetic map. Theor Appl Genet.

- 878 2004;109(3):451-63. Epub 2004/05/29. doi: 10.1007/s00122-004-1653-5. PubMed PMID:
879 15168022.
- 880 44. Bodenes C, Chancerel E, Ehrenmann F, Kremer A, Plomion C. High-density linkage
881 mapping and distribution of segregation distortion regions in the oak genome. *DNA Res.*
882 2016;23(2):115-24. Epub 2016/03/26. doi: 10.1093/dnares/dsw001. PubMed PMID:
883 27013549; PubMed Central PMCID: PMC4833419.
- 884 45. Tirrell AR, Vendrely KM, Checkley LA, Davis SZ, McDew-White M, Cheeseman IH, et al.
885 Pairwise growth competitions identify relative fitness relationships among artemisinin
886 resistant *Plasmodium falciparum* field isolates. *Malar J.* 2019;18(1):295. Epub 2019/08/30.
887 doi: 10.1186/s12936-019-2934-4. PubMed PMID: 31462253; PubMed Central PMCID:
888 PMC6714446.
- 889 46. Anthony TG, Polley SD, Vogler AP, Conway DJ. Evidence of non-neutral polymorphism in
890 *Plasmodium falciparum* gamete surface protein genes Pfs47 and Pfs48/45. *Mol Biochem*
891 *Parasitol.* 2007;156(2):117-23. Epub 2007/09/11. doi: 10.1016/j.molbiopara.2007.07.008.
892 PubMed PMID: 17826852.
- 893 47. Manske M, Miotto O, Campino S, Auburn S, Almagro Garcia J. Analysis of *Plasmodium*
894 *falciparum* diversity in natural infections by deep sequencing. *Nature.*
895 2012;487(7407):375-9. doi: 10.1038/nature11174.
- 896 48. Xu S, Hu Z. Mapping Quantitative Trait Loci Using Distorted Markers. *International Journal*
897 *of Plant Genomics.* 2009;2009:1-11. doi: 10.1155/2009/410825.
- 898 49. Li HW. Aligning sequence reads, clone sequences and assembly contigs with BWA-MEM.
899 arXiv:13033997v2. 2013.

900 50. DePristo MA, Banks E, Poplin R, Garimella KV, Maguire JR, Hartl C, et al. A framework for
901 variation discovery and genotyping using next-generation DNA sequencing data. *Nature*
902 *Genetics*. 2011;43(5):491-8. doi: 10.1038/ng.806.

903

904 **Figure Captions**

905 **Fig 1. Timeline for performing *P. falciparum* crosses in FRG huHep/huRBC mice.** Uncloned
906 F1 progeny from *P. falciparum* genetic crosses of recent field isolates can be recovered in 6
907 weeks from asexual stage culture of parent lines. Cloning of potential F1 recombinant progeny
908 takes an additional 6 weeks. Next generation sequencing of potential recombinant progeny and
909 identification of unique recombinants via our new pipeline takes an additional 6 weeks.

910 **Fig 2. Cloning results and estimated recombinant progeny for each cross.** (A and B)

911 Genotyping results for each cross, clusters denote individual clones of the same genotype. (A)
912 NF54 x NHP4026 contained few selfed progeny and almost all repeat sampling of the same
913 genotype (clusters) occurred with a cloning round, * denotes the only observed repeat sampling
914 event between cloning rounds. (B) MKK2835 x NHP1337 produced many selfed progeny and
915 few instances of repeat sampling of recombinant genotypes all from cloning round 2. (C)
916 Progeny for NF54 x NHP4026 and MKK2835 x NHP1337 cross were filtered to identify unique
917 recombinant progeny (blue). Selfed progeny (orange), non-clonal progeny (grey) and repeat
918 sampling of the same genotype within a cloning round (yellow) and between cloning rounds
919 (black) were filtered out of total genotyped progeny.

920 **Fig 3. Physical maps for crosses.** Physical maps (A & B) depict inheritance patterns in 5KB
921 blocks for each progeny (y axis) across core regions of the 14 nuclear chromosomes (x axis) with
922 black representing the drug susceptible parent and red the drug resistant parent, non-core regions

923 of the genome with no variant calls are shown in grey with yellow showing chromosome
924 boundaries. (A) The physical map for NF54 x NHP4026 shows several regions where haplotype
925 blocks are primarily inherited from either parent and deviate significantly from the expected 1:1
926 ratio. (B) The physical map for MKK2835 x NHP1337 shows more even inheritance ratios
927 across the genome with no significant deviations from expected mendelian ratios.

928 **Fig 4. Segregation Distortion Decreases Power and Mapping Resolution.** (A) Frequency of
929 the NHP4026 SNP alleles in unique recombinant progeny in NF54 x NHP4026 is highly
930 repeatable across biological replicates (black – all progeny, red – progeny from biological
931 replicate 1, blue – progeny from biological replicate 2). Horizontal lines represent significance
932 thresholds (χ^2 $p=0.001$) for segregation distortion for each corresponding set of progeny.
933 Colored regions show significant segregations distortion in both biological replicates. Genes are
934 shown for the most highly skewed sub-regions.

935 **Fig 5. Power analysis for different size progeny sets.** Power curves are shown from simulated
936 phenotypes for NF54 x NHP4026 progeny for different size progeny sets. The top row shows
937 power curves where the phenotype only has a single replicate per progeny strain and the bottom
938 row shows results for 5 replicate phenotype values per progeny strain. The first column shows
939 results for a single locus effect, the second column shows results for an additive 2 loci effect and
940 the third column shows results for an epistatic interaction between 2 loci. The horizontal black
941 line denotes 80% power.

942 **Fig 6. Detecting complex associations.** QTL scans of simulated phenotypes with one major
943 ($ES=0.6$) and two minor ($ES=0.2$ and 0.15) contributing loci for $N=84$ (grey), 60 (blue) and 35
944 progeny (black). The major locus is detected for all sizes of N , but only one minor locus is
945 detected for $N=60$ progeny and neither minor locus is detected at $N=35$ progeny.

946 **Fig 7. Power loss due to segregation distortion.** (A) Effect of SD on mapping power in NF54 x
947 NHP4026 with simulated phenotype data at different effect sizes. Each sub-panel shows the
948 relationship between allele frequency and power for different numbers of progeny at a fixed
949 effect size. For high effect size, allele frequency has little effect on power. At lower effect sizes
950 we observe a large loss of power for alleles with less than 0.3 allele frequency. (B) QTL
951 mapping of CQ IC₅₀ (ES=0.84) in 35 progeny in the NF54xNHP4026 cross results in a LOD
952 score of 18 and a genome wide p-value = 0.000696 showing that in real data with extreme SD a
953 trait with high effect size is detectable.

954

955 **Supporting Information**

956 **S1 Fig. Cloning results for each cross by biological replicate and cloning round.** Cloning
957 success varied as a function of length of time parasites were in bulk culture before cloning. (A)
958 Progeny for the NF54 x NHP4026 cross were filtered to identify unique recombinant progeny
959 (blue). Selfed progeny (orange), non-clonal progeny (grey) and repeat sampling of the same
960 genotype within a cloning round (yellow) and between cloning rounds (black) were filtered out
961 of total genotyped progeny for each biological replicate and cloning round. (B) Progeny for the
962 MKK2835 x NHP1337 cross were filtered to identify unique recombinant progeny (blue). Selfed
963 progeny (orange), non-clonal progeny (grey) and repeat sampling of the same genotype within a
964 cloning round (yellow) and between cloning rounds (black) were filtered out of total genotyped
965 progeny for each cloning round.

966 **S2 Fig. Segregation distortion in all published *P. falciparum* crosses.** Allele frequencies
967 plotted across the genome for all 6 published *P. falciparum* crosses show no significant

968 segregation distortion in the MKK2835xNHP1337 cross (A) in contrast to all other published
969 crosses which show regions of significant segregation distortion (B-F).

970 **S3 Fig. Mapping Resolution for different size progeny sets.** Average mapping resolution
971 reported as number of genes per 1.5 LOD interval for simulated phenotypes that accurately map
972 to the 1.5 LOD interval surrounding the causal loci. Progeny set size varied from the full NF54 x
973 NHP4026 progeny set of 84 and was subsampled at 30, 40, 50, 60 and 70 progeny. Each curve
974 represents phenotypes simulated with a given effect size (ES) with ES ranging between 0.1 to
975 0.8.

976 **S4 Fig. Nonclonal Progeny Heatmap.** Heatmap showing regions of the genome for each
977 progeny with above expected numbers of heterozygous allele calls. Regions with above expected
978 heterozygous SNP calls were identified through a sliding window analysis. Progeny along with
979 an uncloned sample (denoted with an *) are shown as rows and each column represents a 90kb
980 region (window size was defined as the expected distance between heterozygous SNP calls based
981 on the heterozygous SNP call rate for each cross). (A) In progeny of the NF54 x NHP4026 cross,
982 25 progeny had regions with above expected heterozygosity. (B) In progeny of the MKK2835 x
983 NHP1337 cross, 35 progeny had regions with above expected heterozygosity. The un-cloned
984 samples (*) show above background heterozygosity or high heterozygosity across the genome.

985 **S1 Table. Mosquito stage crossing results.**

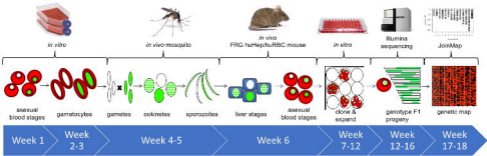
986 **S2 Table. Cloning methodology and results.**

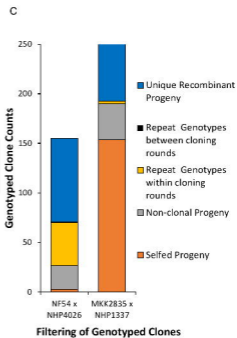
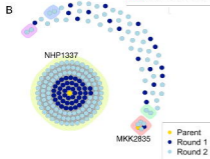
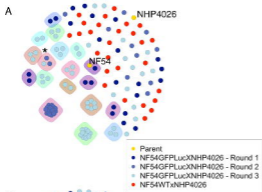
987 **S3 Table. NF54/NF54-GFPLuc x NHP4026 Genetic Map**

988 **S4 Table. MKK2835 x NHP1337 Genetic Map**

989 **S5 Table. Allele frequencies and significance of segregation distortion in NF54 x NHP4026**
990 **progeny.**

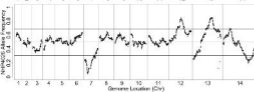
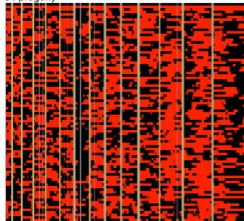
991 **S6 Table. Microsatellite information.**



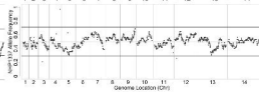
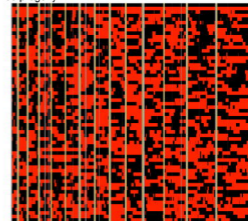


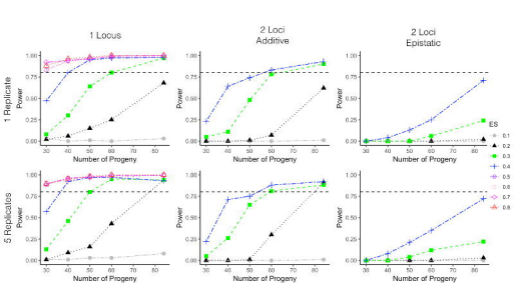
A NF54 x NHP4026

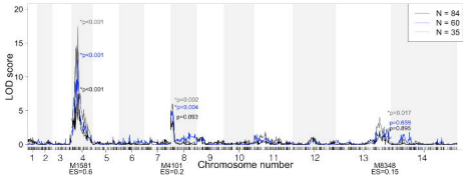
84 progeny

**B** MKK2835 x NHP1337

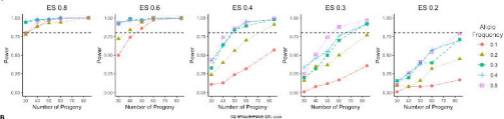
60 progeny



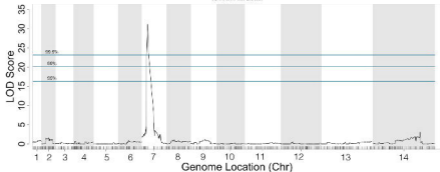




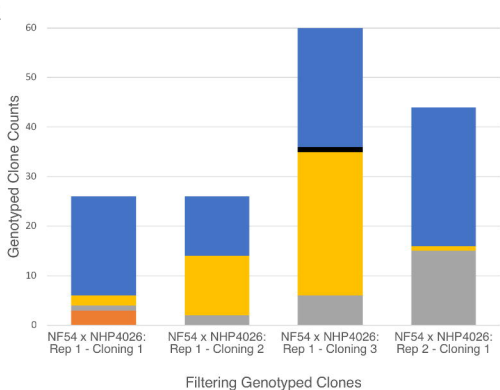
A



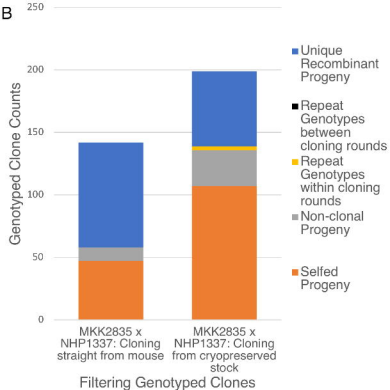
B

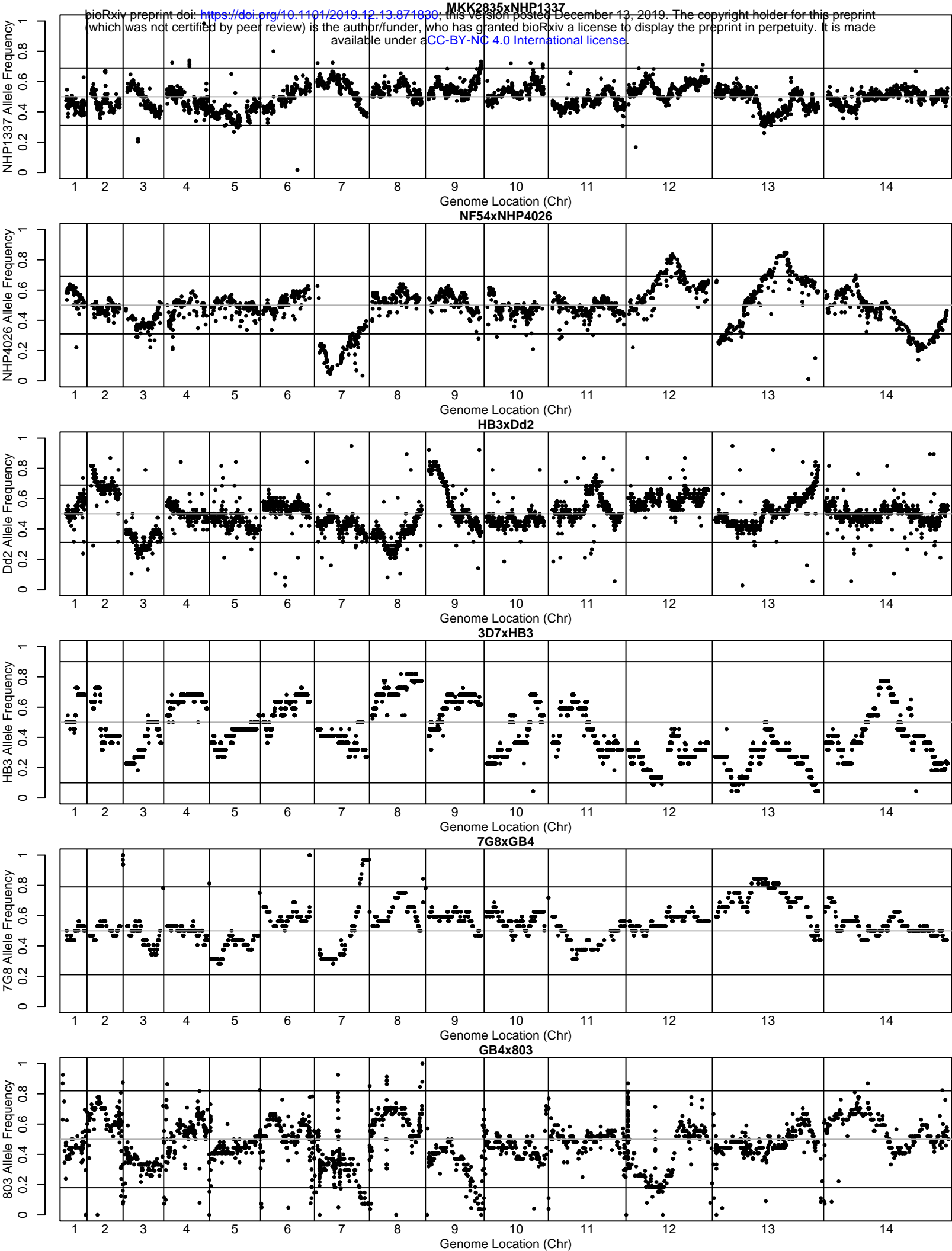


A

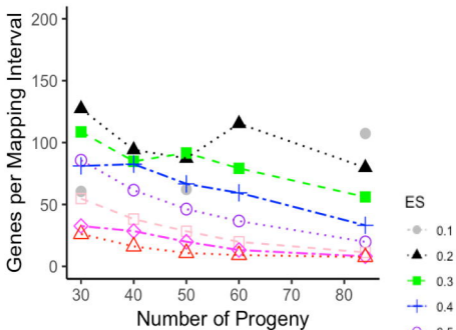


B

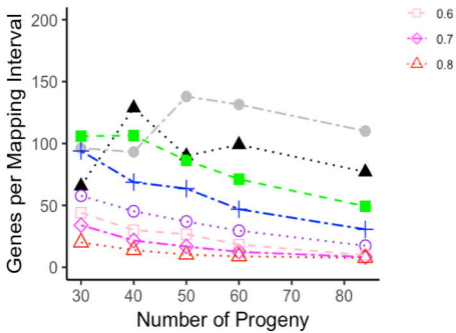




1 Replicate

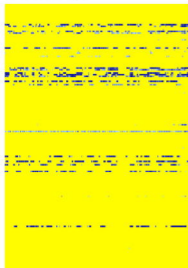


5 Replicates



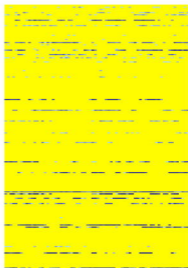
A

NF54 x NHP4026



B

MKK2835 x NHP1337



- background error
- above background heterozygosity
- high heterozygosity